Soil Dynamics and Earthquake Engineering 119 (2019) 220–234

Contents lists available at ScienceDirect

Soil Dynamics and Earthquake Engineering

journal homepage: www.elsevier.com/locate/soildyn

Vibration isolation using 3D cellular confinement system: A numerical investigation

K.N. Ujjawal, H. Venkateswarlu, A. Hegde*

Department of Civil and Environmental Engineering, Indian Institute of Technology Patna, 801103, India

ARTICLE INFO

Keywords:
Machine induced vibrations
Geocells
Vibration isolation
Block resonance test
FLAC^{3D}
Dynamic properties

ABSTRACT

This paper investigates numerically the potential use of cellular confinement systems in isolating the machine induced vibrations. The numerical analysis was carried out using the three dimensional explicit finite difference package FLAC^{3D}. Primarily, the numerical model was validated with the results of field resonance tests, performed on the foundation beds reinforced with and without cellular confinement systems. The 3D cellular confinement was simulated using two techniques, namely, Equivalent Composite Approach (ECA), and Honeycomb Shape Approach (HSA). The isolation efficiency of the confined cell was determined in terms of the reduction in displacement amplitude, peak particle velocity, and the improvement in elasticity of the foundation bed. From the results, 56% reduction in displacement amplitude was observed in the presence of geocell reinforcement. Similarly, 42% change of resonant frequency was observed as compared to the unreinforced condition. The elasticity of the foundation bed was improved by 102% with the provisions of geocell. Further, it was noticed that the modelling of geocell through the HSA approach provided the accurate prediction of the experimental results. With the help of HSA technique, the effect of confinement area and the height of geocell in reducing the amplitude of vibration was investigated. Further, the parametric study was conducted to investigate the effect of different geocell properties on the dynamic behaviour of reinforced foundation bed. The parametric study results revealed that the geocell modulus and the interface friction angle directly influence the performance of geocell reinforced bed under dynamic loading condition.

1. Introduction

The design of foundations for dynamically loaded structures has become a great interest in the field of geotechnical engineering. The foundations are often subjected to dynamic loads due to the many circumstances, such as traffic loads, earthquakes, and the machine vibrations. The major problem associated with these dynamic loads is ground-borne vibration. One of the classical examples is the Machine foundations. The emanated vibrations from the machines transfer to the soil through the foundations. The transmitted vibrations may exhibit adverse effect on the superstructure and the supporting soil. Moreover, these dynamic motions are responsible for the unsatisfactory functioning of the machine and the nearby equipment. The adverse effect on the performance of foundation bed can be prevented by enhancing the dynamic properties of the soil, namely, dynamic shear modulus, and the elasticity of the foundation bed. Apart from the parameters mentioned above, preventing the resonance of a system is also essential for the safe functioning of such foundations.

The ground motion characteristics of the vibration energy are significantly influenced by the excitation frequency, and the type of wave induced from the vibration source. After the pioneering work of Woods [1], the installation of wave barriers has gained popularity for mitigating the machine-induced vibrations through the active and passive modes [2,3]. Several studies [4–9] highlighted the various geometrical aspects of open trenches in isolating the machine-induced vibrations through experimental and analytical approaches. The maintenance problems posed by the open trenches led to the installation of infilled trenches. The performance of different infill materials on the isolation performance of infilled trenches has been investigated [5–17]. The isolation efficiency of infilled trenches are also compared with the performance of open trenches [18–23]. From the reported literature, it was identified that the open and in-filled trenches are effective in controlling the surface (Rayleigh) waves induced from the vibration sources. However, the implementation of these techniques required the excavation and transfer of huge quantities of soil from the site to some other location. On the other hand, such techniques are not feasible in urban areas. Sometimes, excavation may also leads to ground subsidence and damage to the adjacent structures.

* Corresponding author.
E-mail addresses: kumar.mtce16@iitp.ac.in (K.N. Ujjawal), hasthi.pce16@iitp.ac.in (H. Venkateswarlu), ahegde@iitp.ac.in (A. Hegde).

https://doi.org/10.1016/j.soildyn.2018.12.021
Received 14 August 2018; Received in revised form 13 November 2018; Accepted 18 December 2018

List of symbols

A	contact area of the footing with the soil mass (m^2)
A_{rf}	amplitude reduction ratio (dimensionless)
b	width of the geocell mattress (m)
B	width of the footing (m)
C	cohesion (kPa)
c_i	interface cohesion (kPa)
C_r	increase in apparent cohesion (kPa)
C_u	coefficient of elastic uniform compression (MN/m^3)
C_τ	coefficient of elastic uniform shear (MN/m^3)
C_ϕ	coefficient of elastic non-uniform compression (MN/m^3)
C_Ψ	coefficient of elastic non-uniform shear (MN/m^3)
d	equivalent pocket diameter of the geocell material (m)
d'	diameter of cell pocket at ξ_a axial strain (m)
e	eccentric distance between centre of mass and the centre of rotation (m)
ECA	equivalent composite approach
E	Young's modulus (MPa)
E_c	modulus of elasticity of concrete (MPa)
f_{nz}	natural frequency of the foundation soil system (Hz)
f_r	resonant frequency of the foundation soil system (Hz)
$F(t)$	dynamic force excited over the footing in a vertical mode (N)
F_o	total unbalanced dynamic force excited over the footing (N)
F_{ir}	frequency improvement ratio (dimensionless)
F_r	resonant frequency of the reinforced soil system (Hz)
F_u	resonant frequency of the unreinforced soil system (Hz)
G	shear modulus (MPa)
G_s	specific gravity of foundation soil (dimensionless)
HSA	honeycomb shape approach
H	height of the geocell layer (m)
k_i	interface shear modulus (MPa/m)
K_p	coefficient of passive earth pressure (dimensionless)
K	stiffness of the soil (MN/m)
M	mass of the vibrating block, oscillator and motor (kg)
m_e	eccentric mass weight (kg)
N	standard penetration test corrected-n values
PPV	peak particle velocity (mm/s)
r_0	equivalent radius of the non-circular footing (m)
t	dynamic time (s)
t_i	thickness of geocell (mm)
u_c	depth of placement of the geocell from the ground surface (m)
ω	circular natural frequency in cycles (rotations) per minute
X_m	resonant displacement amplitude (mm)
γ_c	unit weight of concrete (kN/m^3)
γ_d	unit weight of the foundation bed (kN/m^3)
ρ	density of subsurface soil layers (g/cc)
φ	angle of shearing resistance (°)
φ_i	interface friction angle (°)
ν	Poisson's ratio (dimensionless)
ν_c	Poisson's ratio of concrete (dimensionless)
θ	eccentricity angle (°)
ξ_a	axial strain in the geocell material (dimensionless)
ξ_c	circumferential strain in the geocell material (dimensionless)
$\Delta\sigma_3$	increase in the confining pressure on infill material (kPa)

Currently, the application of reinforced earth has become popular over other conventional ground improvement techniques for improving the stability of the foundation bed. Among several types of reinforcing materials, geosynthetics have found to be most economical and advantageous under monotonic and cyclic loading conditions [24–27]. However, very limited investigation has been carried out to understand the probable benefits of geosynthetics in enriching the performance of machine foundation. Boominathan et al. [28] investigated the effectiveness of the reinforced earth under the machine vibrations. The study was carried out by performing a series of field block resonance tests over the reinforced soil bases with different types of planar reinforcements. The results revealed that the resonant amplitude was reduced by 67% in the presence of the pretensioned wire grid. Similarly, the maximum improvement in the resonant frequency of the foundation bed was observed due to the provision of high tensile wire grid. Clement et al. [29] studied the performance of geogrid in improving the dynamic properties of the foundation bed through the model resonance tests. The dynamic shear modulus was improved by 30%, when the foundation bed was reinforced with the geogrid reinforcement. The laboratory block resonance test conducted by Sreedhar and Abhishek [30] has also revealed a significant reduction in resonant amplitude in the presence of geogrid reinforcement.

As observed from the available studies, there is a lack of studies to understand the efficacy of the 3D cellular confinement system (also known as Geocells) in isolating the machine induced vibrations. A few numerical studies have been carried out to highlight the confinement effect in improving the machine foundation performance. Azzam [31] has studied the vibration isolation efficacy of the confined cell using two-dimensional finite element package, PLAXIS2D. The results revealed that 230% improvement in the subgrade damping and 75% reduction in displacement amplitude due to the provision of the confined cell under machine foundation. Venkateswarlu and Hegde [32] investigated the performance of geocell reinforced bed with different infill materials under the machine induced vibration through PLAXIS2D. Three different infill materials, namely, sand, red soil, and aggregate were used for the numerical analysis. A significant improvement in the stiffness and the natural frequency of the foundation soil system was observed in case of geocell with aggregate as infill material.

The numerical simulation of the geocell reinforcement has evolved with time. The Equivalent Composite Approach (ECA) was among the first few techniques of modelling geocell. Being a simple technique, it is frequently adopted to model geocells. According to ECA, the geocell and its infill material is modelled as a composite soil layer with enhanced stiffness and strength properties [33,34]. Bathurst and Karpurapu [35] and Rajagopal et al. [36] have provided formulation for the determination of the properties of composite layer. Later on, this technique was adopted by many researchers [37–39] for analysing the performance of geocell reinforced system. Further, some of the researchers have modelled geocell with square shaped pockets [40–42]. Yang et al. [43] and Hegde and Sitharam [33,44,45] have successfully demonstrated the modelling of the actual curvature of the geocell pockets using three-dimensional finite difference package $FLAC^{3D}$. Hegde and Sitharam [33] suggested that modelling the geocell in square shape leads to the non-uniform distribution of the stresses at the corners of the square box. Whereas, the modelling with actual honeycomb shape helps in uniform stress distribution through the periphery of the geocell reinforcement.

In the present study, the effectiveness of the geocell reinforced beds in isolating the machine induced vibrations has been numerically investigated. The numerical investigation has been carried out using the explicit finite difference package $FLAC^{3D}$. Initially, the numerical model was validated with the results of large scale block resonance test. The performance of two different approaches, namely, Equivalent Composite Approach (ECA), and Honeycomb Shape Approach (HSA) in predicting the behaviour of geocell-reinforced condition has been

compared. Though the manuscript emphasizes on the numerical simulation, the results of the field block resonance tests also have been discussed.

2. Field vibration tests

Primarily, large-scale block resonance test was carried out to understand the efficacy of the cellular confinement system in isolating the machine induced vibrations. The schematic representation of the block resonance test is shown in Fig. 1(a). The major components of the test setup include concrete block, mechanical oscillator, DC Motor, speed control unit, and the vibration meter with piezoelectric accelerometer. The M20 grade concrete block of 600 mm × 600 mm × 500 mm (length × width × depth) was used. It was placed centrally over the prepared foundation bed with and without geocell reinforcement.

The mechanical oscillator was used to induce the rotating mass type excitation over the foundation. It can emanate the dynamic excitation as similar to the high speed rotary machine. The oscillator was mounted over the machine foundation through the bolting arrangement. The DC motor of 6 HP capacity was used to regulate the dynamic force induced from the oscillator. The operating frequency of the motor was determined using speed control unit through digital technique. It can measure the frequency of a rotating body with the help of non contact speed sensor. The speed control unit consists of digital counter circuit to count the frequency in terms of RPM based on the electrical pulse received from the sensor. One end of the sensor was fixed nearer to the rotating body and the other end connected to the speed control unit. The maximum sensing range of the sensor is 10,000 RPM with a resolution of 1RPM. It is capable of working from a distance of 2 mm from the objects. In this study, it was placed at a distance of 1.5 mm from the MS stud (attached to the rotating shaft) of the motor. The photographic representation of the arrangement of the sensor during the field test is shown in Fig. 1(b). The various researchers have adopted the similar procedure for measuring the frequency of the vibration systems [74,76]. During the test, the vibration parameters such as displacement amplitude and the velocity were recorded using digital vibration meter with the help of accelerometer.

The block resonance test was conducted in a vertical mode over the prepared foundation bed of 2 m × 2 m × 0.5 m. The dimensions of the foundation bed was selected based on the past studies. Raman [75] has investigated the effect of test pit size on the dynamic response of the system. The test pits of lengths 3.3*D* and 4.6*D* (where *D* is the diameter of the footing) were considered. The identical nature of the dynamic response was observed from both the pits. Further, IS 5249 [77] recommends that the ratio between the width of the test pit to the width of the machine foundation is three for conducting the block vibration test. Boominathan et al. [28] studied the dynamic response of foundation bed by considering the test pit size 3 times the width of the machine foundation. Hence, in the present study, the width of the foundation bed was considered equal to the 3.3 times the width of machine foundation. The foundation bed was prepared with the locally available soil having the fines content of 16%. It was classified as silty sand (SM) based on the Unified Soil Classification System. The particle size distribution of the foundation soil is shown in Fig. 2(a). The compaction parameters of the foundation soil were determined from the Standard Proctor test. The variation in dry density with the change in water content is shown in Fig. 2(b). From the figure, the optimum moisture content was observed as 12.6%. The subsurface profile of the test location is shown in Fig. 3a–c. It was identified that the subsurface consisted of silty sand (SM) up to a deeper depth at the test site. The top

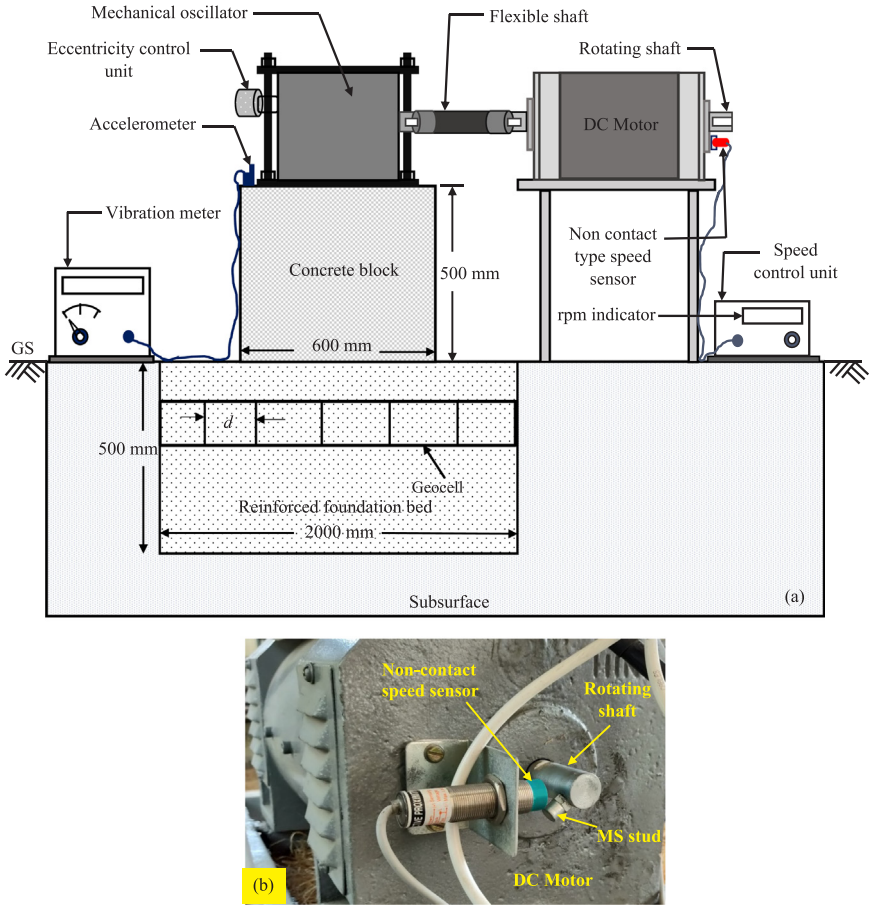

Fig. 1. Block vibration test setup: (a) schematic representation; (b) arrangement of the non-contact speed sensor.

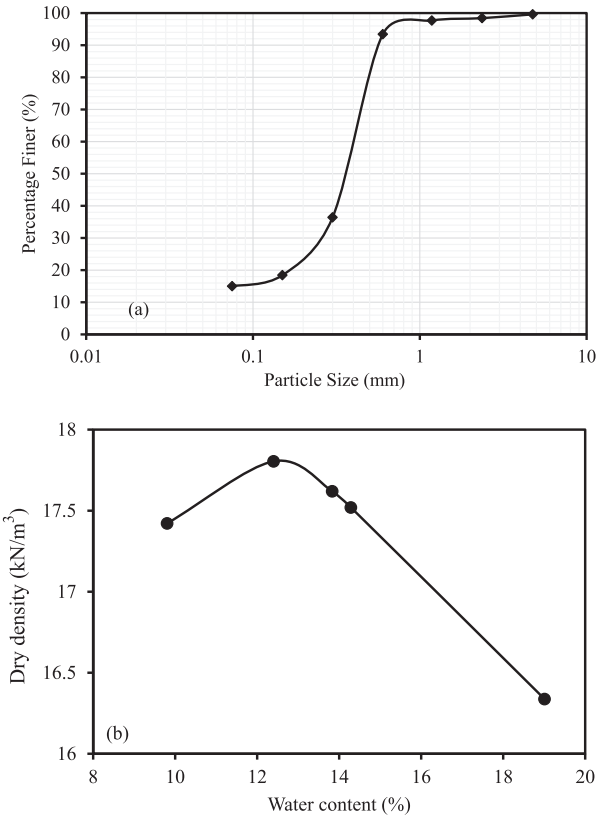

Fig. 2. Foundation soil properties: (a) particle size distribution; (b) dry density versus water content response of foundation soil.

0.5 m of foundation soil was reconstituted with the same material to place the foundation block. The brief description about the classification of soil strata and the determination of different parameters are described in numerical modelling.

The total depth of the foundation bed was prepared with ten numbers of layers, having the thickness of 50 mm each. Each layer was compacted at the optimum moisture content of the soil (as shown in Table 1) with the compaction effort of 593 kJ/m^3. To verify the achieved dry density, core cutter samples were collected from the different locations of the foundation bed. The average dry density and moisture content of the foundation bed was observed as 17.45 kN/m^3 and 12.5% respectively. The similar procedure was followed for the preparation of both unreinforced and geocell reinforced conditions. The geocell used in the present study was made up of Novel Polymeric Alloy (NPA) material. The stress-strain response of the geocell reinforcement used in the present study is shown in Fig. 4. It was determined from the tensile strength test based on the recommendations of ASTM D-4885 [46]. The properties of the foundation soil and the geocell reinforcement were summarized in the Table 1.

Table 1
Properties of the foundation soil and geocell.

Parameter	Value
Foundation soil	
Classification	Silty Sand (SM)
Specific Gravity, G_s	2.64
Unit weight, γ_d (kN/m^3)	17.9
Optimum moisture content (%)	12.6
Geocell	
Material	Neoloy (NPA)
Cell depth (mm)	120
Cell length (mm)	245
Cell width (mm)	210
Number of cells/m^2	39
Strip thickness (mm)	1.53
Cell wall surface	Perforated
Density (g/cm^3)	0.95 (± 1.5%)
Cell seam strength (N)	2150 (± 5%)

The geocell was placed at a depth of 0.1B (where B is the width of the footing) from the ground surface [26,27,34,37,39,67,78,79]. The width of the geocell was considered as similar to the width of the foundation bed (i.e., 3.33B). The foundation soil (silty sand) was used as the infill material for filling the pockets of geocell reinforcement. Initially, first two rows of the geocell layer were filled up to half height

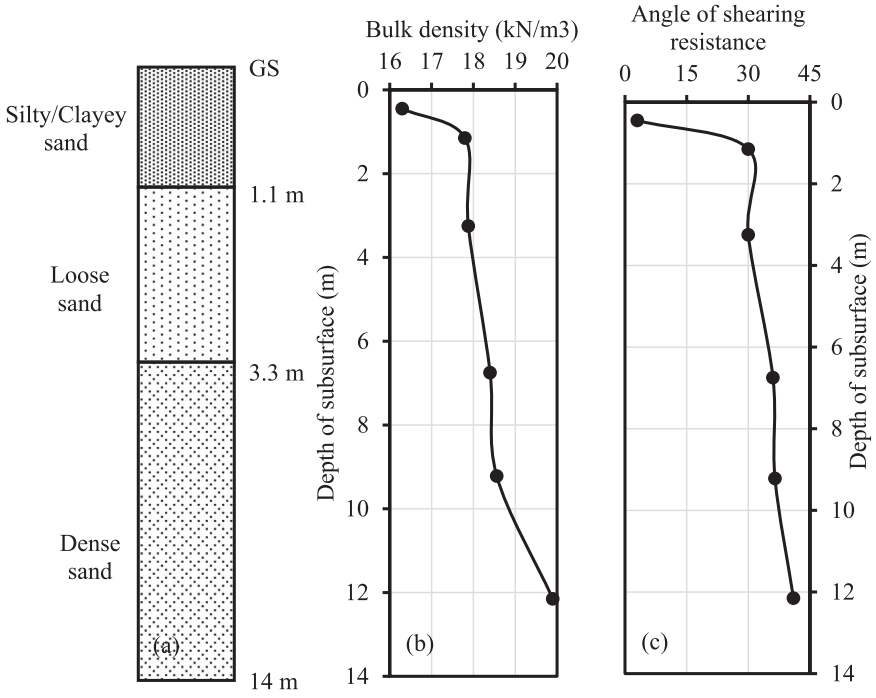

Fig. 3. Subsurface details: (a) profile of the bed; (b) change in bulk density; (c) variation in angle of shearing resistance.

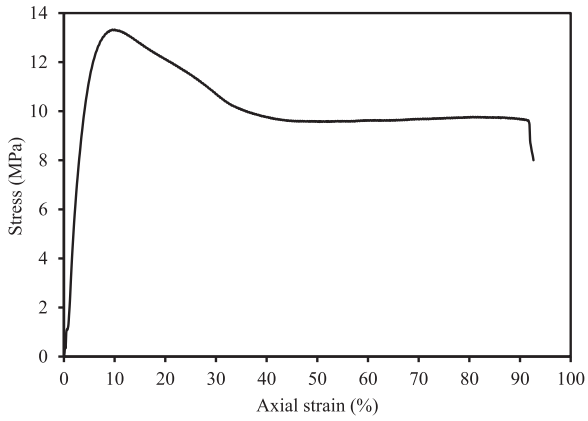

Fig. 4. Stress–strain behaviour of the geocell reinforcement.

before filling the first layer to its full height. The similar sequence was continued to fill the complete portion of the geocell layer. Upon filling of all the geocell pockets, the top layer with a thickness of 60 mm was provided. The photographs of the preparation of foundation beds are shown in Fig. 5.

3. Numerical modelling

3.1. Numerical model (meshing, boundary conditions and material properties)

In the present study, numerical analysis was carried out using the Fast Lagrangian Analysis of Continua in three-dimensions (FLAC^{3D}). It was selected due to its capability of simulating the complex behaviour of various geotechnical problems under static and cyclic loading conditions. Several studies in the past have used FLAC for analysing the dynamic response of foundation beds under the machine induced vibrations. Haldar and Sivakumar Babu [70] compared the dynamic response of foundation bed reinforced with metallic bars obtained from the experimental study using FLAC2D. Ghosh [71] studied the dynamic interference of two closely spaced machine foundations through FLAC3D. The several studies have reported the efficacy of FLAC in studying the behaviour of geosynthetics reinforced foundation beds under static and dynamic loading conditions [27,33,34,39,44,45,51,72]. Thus, in this study FLAC^{3D} was used for the numerical investigation. It uses an explicit finite difference formulation for obtaining the solution of initial and boundary value problems. It consists of different built-in constitutive models, and structural elements (SELs) for modelling the wide variety of soil behaviour, geomaterials and reinforcements. The SELs are used to model the different structural components, namely, beams, cables, piles, shells, geogrids and the liners. It is also equipped with the interface elements to simulate the interface behaviour between two distinct materials like, faults in the rocks, and the interface between soil and geosynthetics. Further, FLAC^{3D} contains a powerful built-in programming language called FISH (FLACish) for analysing and defining the new variables and functions.

The existing subsurface profile significantly influences the dynamic response of the foundation soil system [47]. Hence, in the present study, the existing subsurface profile at the test site was considered into account for simulating the vibration tests using FLAC^{3D}. The variation in subsurface was investigated using the Standard Penetration Test (SPT) data. Initially, the obtained SPT-*N* values were corrected to 60% energy as per the recommendations of Skempton [48]. The corrected SPT-*N* values revealed that the subsurface consists of three different layers, namely, silty/clayey sand, loose sand, and dense sand from the ground surface. The different properties of the individual soil layers were determined through the laboratory tests. The variation in subsurface profile with their properties, and the change in corrected *N* value with the depth is presented in Fig. 6a–b. The Poisson's ratio (ν) value of 0.3 was considered for the soil layers across the depth [49]. The Young's modulus (E) of the subsurface soil layers were determined using the corrected SPT-*N* values as per the recommendations of Bowles [50]. The elastic modulus for the existing soil layers can be determined by,

$$\text{For Silty Clay: } E = 300(N + 6) \tag{1}$$

$$\text{For Sand: } E = 7000\sqrt{N} \tag{2}$$

where N is the corrected SPT-*N* value and E is obtained in kPa. Further, the elastic modulus calculated from the SPT data was converted to their respective dynamic modulus [66,81]. The Alpan [66] has proposed the empirical curves to convert the elastic modulus to the dynamic modulus. Also, Wichtmann and Triantafyllidis [81] proposed the correlation between static modulus (obtained from triaxial tests) and dynamic modulus (from resonant column tests) for non cohesive soils. These dynamic modulus values for different soil layers has been presented in Fig. 6a. The same values were employed for the numerical simulation purpose.

In the present study, the subsurface was modelled with three numbers of individual soil layers [68,69,71]. The Mohr Coulomb constitutive behaviour was used to similate the behaviour of subsurface instead of Gibson soil model. The study of Mbawala [69] reported that the change in dynamic response of machine foundation was

Fig. 5. Preparation of foundation bed: (a) excavated test pit; (b) partially filled geocell reinforcement.

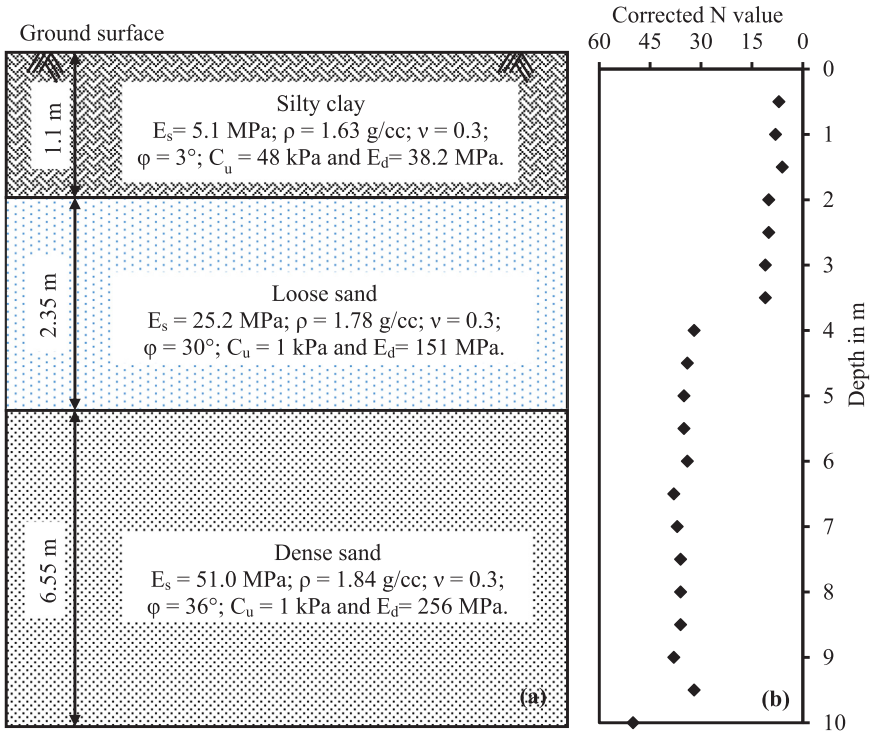

Fig. 6. Details of the subsurface profile: (a) soil profile; (b) variation in corrected SPT-*N* value with the depth.

insignificant while modelling the subsurface through Gibson soil model and homogeneous soil layer. The various researchers have considered the constant elastic modulus for the entire depth of individual soil layer while modelling the subsurface profile [68,71]. Thus, the modulus of the individual soil layers was maintained constant in the numerical analysis. Initially, the preliminary analysis was carried out to understand the effect of boundary location on the dynamic response of the reinforced soil system. From the preliminary analysis, the complete dissipation of vibration energy was observed at the distance of 12*B* from the footing face. Hence, the dimension of the numerical model was selected as 15 m × 15 m × 10 m. The sensitivity analysis was performed to determine the optimum mesh size (density) for the model in the present study. It was carried out by varying the number of zones of the numerical model. The displacement amplitude of the geocell reinforced foundation bed at the resonant frequency of eccentricity angle 20° was considered for the analysis. The variation in amplitude of the vibration with the change in number of zones of the model is shown in Fig. 7. It was noticed that the increase in amplitude of the vibration with the increase in number of zones. The increment in amplitude was found negligible when the number of zones beyond 18,000. Hence, the number zones were considered as 18,000 to simulate the geocell reinforced machine foundation bed. The brick element was used to model the subsurface and the machine foundation. The dimension of the foundation bed was considered as similar to the experimental study. Over the simulated foundation bed, the machine load was applied. The Mohr-Coulomb constitutive behaviour was considered to simulate the foundation soil. Several researchers [51–53] have been used the similar constitute behaviour for the simulation of the problems subjected to the dynamic loading conditions. The concrete footing was modelled as a linear elastic material. In order to simulate the vibration decay in the soil system, 5% material damping was considered for all the soil layers [54]. The displacement was restrained in all the three directions at the bottom plane of the model. Whereas, it was allowed in vertical direction and restrained in horizontal directions at the vertical faces of the model. In order to simulate the far field response of the site, quiet boundaries were applied to the extreme (vertical and horizontal) boundaries of the numerical model. It helps in minimizing the wave reflections into the system from the model boundaries. In the present study, the geocell mattress was simulated by using two modelling techniques, namely, Equivalent Composite Approach (ECA), and Honeycomb Shape Approach (HSA). In both the techniques, the width and the depth of placement of geocell was considered as similar to the experimental study. The developed FLAC^{3D} finite difference models for different reinforced cases with the subsurface profile are shown in Fig. 8a–c.

In the present study, the performance of unreinforced and geocell reinforced conditions were analysed under the application of vertical mode rotating mass type excitation. The relationship between total vertical harmonic excitation applied over the footing in terms of eccentricity angle (θ) and magnitude of the vertical unbalanced force (F_0) is given by,

$$F\left(t\right) = F_0 \sin\left(\frac{\theta}{2}\right) \tag{3}$$

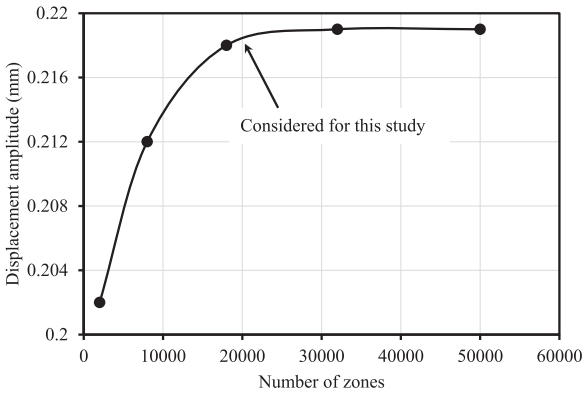

Fig. 7. Variation in displacement amplitude with the increase in number of zones.

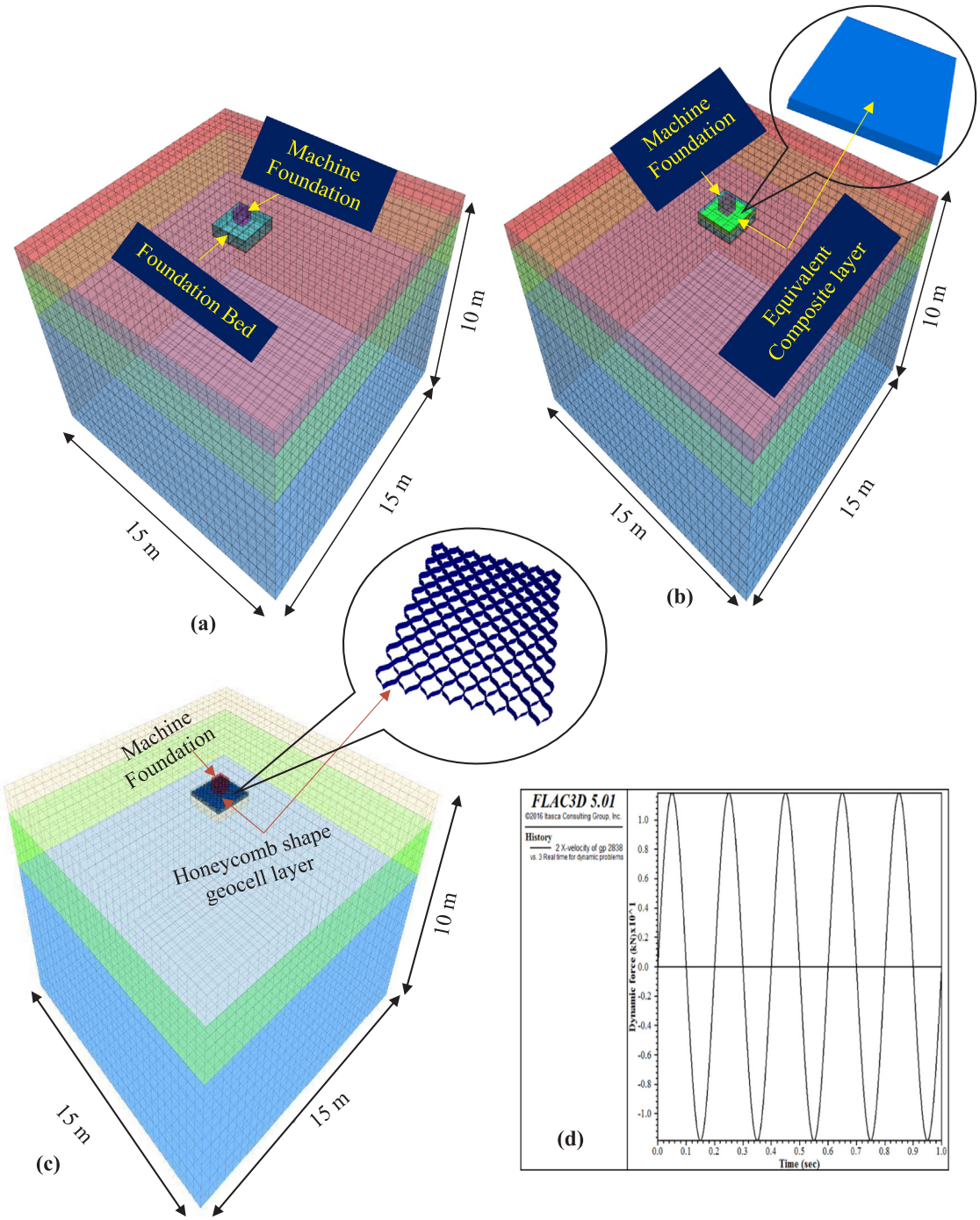

Fig. 8. FLAC^{3D} finite difference model for different conditions: (a) unreinforced; (b) geocell reinforced-ECA; (c) geocell reinforced-HSA; (d) typical loading pattern.

$$F_0 = m_e e\omega^2 \quad \left(m_e = \frac{W_e}{g}\right) \tag{4}$$

$$F(t) = \frac{W_e}{g} e\omega^2 sin\left(\frac{\theta}{2}\right) \tag{5}$$

where $F(t)$ is the vertical component of the total dynamic force in N, F_0 is the total unbalanced dynamic force excited over the footing in N, *We* is the eccentric weight in the oscillator in kg, e is the eccentricity (radius) of the rotating mass in the oscillator in m, ω is the circular natural frequency in cycles (rotations) per second, t is the dynamic time in s and g is the acceleration due to gravity in m/s^2. The detailed description pertaining to the derivation of above mentioned formulae is reported by Richart et al. [54] and Das [80]. The frequency of the dynamic excitation was varied from 5 Hz to 45 Hz with an increment of 5 Hz. The input dynamic motion applied over the machine foundation corresponding to the frequency of 5 Hz is shown in Fig. 8d.

The properties of different materials used in the numerical analysis have been summarized in the Table 2. The direct shear test was performed to determine the shear strength properties of the foundation soil. The Young's modulus (E) of the foundation soil was determined through the consolidated undrained triaxial compression test. Alternatively, the realistic dynamic modulus obtained from resonant column test may also be used in the simulations. The shear and bulk modulus of the equivalent composite layer was borrowed from the studies of Latha and Somwanshi [37], and Hegde and Sitharam [33]. The dilatancy

Table 2
Properties of different materials used in numerical modelling.

Material	Parameter	Value
Foundation soil (Silty sand)	Unit weight, γ_d (kN/m^3)	17.45
	Angle of shearing resistance, φ (°)	32
	Cohesion, C (kPa)	1
	Young's modulus, E (MPa)	20
	Poisson's ratio, ν	0.3
Concrete footing	Modulus of elasticity of concrete, E_c (MPa)	2×10^4
	Unit weight of concrete, γ_c (kN/m^3)	24
	Poisson's ratio of concrete, ν_c	0.15
Geocell-soil composite layer (Equivalent Composite Approach)	Cohesion (kPa)	33
	Internal friction (°)	32
	Poisson's ratio, ν	0.3
	Shear modulus, G (MPa)	25
	Bulk Modulus, K (MPa)	50
Geocell (Honeycomb Shape Approach)	Young's modulus, E (MPa)	275
	Poisson's ratio, ν	0.45
	Thickness, t_i (mm)	1.53
	Interface shear modulus, k_i (MPa/m)	2.36
	Interface cohesion, c_i (kPa)	0
	Interface friction angle, φ_i (°)	30

parameter of the soil was considered as 2/3rd of the angle of internal friction as suggested by [33,37]. The value of the Poisson's ratio (ν) of the foundation soil was borrowed from Bowles [50]. The unit weight, modulus of elasticity, and the Poisson's ratio of the concrete footing were considered from the guidelines of IS: 456 [61]. The modified direct shear test was performed in accordance with ASTM D-5321 [62] to determine the interface shear properties between the geocell and infill material. Itasca [63] and Hegde and Sitharam [45] suggested an interface shear modulus (k_i) of 2.36 MPa/m for the geocells. The Young's modulus of the geocell reinforcement was determined from the tensile stress-strain curve as shown in Fig. 4.

3.2. Equivalent Composite Approach (ECA) of modelling geocells

As per ECA, the geocell and its infill material was modelled as an equivalent composite soil layer with improved strength and stiffness parameters. The performance of the geocell reinforced bed is majorly depends upon the mobilization of additional confinement pressure under cyclic loading conditions [55]. Currently, various models [35,36,56,57] are available for the determination of mobilized confinement in the presence of geocell reinforcement. However, in this study, the simple model proposed by Henkel and Gilbert [58] has been used for the determination of the increase in confinement as given below.

$$\Delta\sigma_3 = \frac{2M\xi_c}{d'}\frac{1}{1-\xi_a} = \frac{2M}{d}\left[\frac{1-\sqrt{1-\xi_a}}{1-\xi_a}\right] \tag{6}$$

Where ξ_a is the axial strain at failure, ξ_c is the circumferential strain in the geocell, d' is the diameter of cell pocket at axial strain ξ_a, M is the secant modulus of the geocell material corresponding to axial strain ξ_a, d is the equivalent diameter of the geocell pocket opening. The similar approach has been adopted by various researchers [34,37,59,60] for modelling the geocell reinforcement. The studies conducted by Bathurst and Karpurapu [58] and Rajagopal et al. [36] suggested that the cohesion value of composite layer increases without any change in the angle of shearing resistance. The increase in cohesion of the equivalent composite layer with the increase in confinement pressure was determined using the equation proposed by Rajagopal et al. [36]. It can be determined by,

$$C_r = \frac{\Delta\sigma_3}{2}\sqrt{K_p} \tag{7}$$

$$K_p = \frac{1+\sin\varphi}{1-\sin\varphi} \tag{8}$$

where C_r is the increase in cohesion due to the increase in the confining pressure ($\Delta\sigma_3$), K_p is the coefficient of passive earth pressure (depends on the internal friction angle (φ) of the infill material). The developed equivalent composite layer is shown in Fig. 8b. It was modelled as to follow elastic-perfectly plastic Mohr-Coulomb failure yield criterion. The various properties of geocell-soil composite layer have been summarized in the Table 2.

3.3. Honeycomb Shape Approach (HSA) of modelling geocells

Honeycomb Shape Approach (HSA) is a complicated and realistic approach for modelling the geocell reinforcement. It involves the consideration of the actual curvature of the geocell pockets. Also, HSA facilitates to simulate the geocell and the infill material with two different constitutive behaviours to represent the actual field scenario. The photograph of the expanded geocell was digitized to obtain the coordinates of the actual curvature. The obtained coordinates were used to model the 3D honeycomb shape of the geocell in FLAC^{3D}. Yang et al. [43] and Hegde and Sitharam [33,34,45] have also adopted a similar approach for modelling the geocell reinforcement. The geogrid structural element available in FLAC^{3D} was used to model the geocell reinforcement. The developed actual honeycomb shape of the geocell reinforcement using the HSA technique is shown in Fig. 8c.

The linear elastic and Mohr Coulomb constitutive models were used to simulate the behaviour of geocell and infill material, respectively. The joint strength of the geocell was maintained by fixing the nodes at

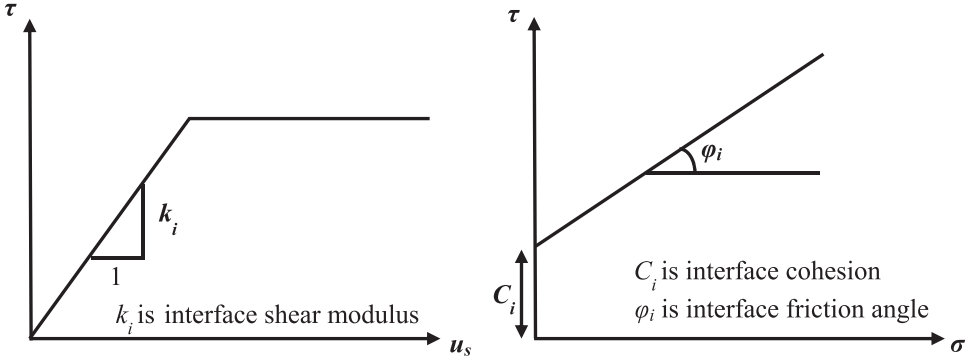

Fig. 9. Interface shear behaviour between geocell and infill material [63,45]: (a) shear stress (τ) versus shear displacement (u_s); (b) shear stress (τ) versus normal stress (σ).

their joints. The other important mechanism offered by the geocell reinforcement is the interface shear behaviour. The interface shear relationship between the geocell and the infill material was considered as linear with Mohr-Coulomb failure criterion as shown in Fig. 9.

The method adopted for analysing the present dynamic problem follows three major steps. Initially, the concrete footing was simulated over the foundation bed and the static stress was applied. The magnitude of static stress was equal to the stresses generated due to self-weight of footing and machine parts. In the second stage, vertical dynamic excitation was applied by considering the dynamic time interval of 10 s. The FISH programming language was used for simulating the dynamic excitation over the machine foundation. It replicates the vibrations induced from the machine in the real field scenario. The analysis was continued by changing the frequency of the dynamic excitation as discussed in the experimental program. These vibrations are transmitted into the soil through the footing. In the third stage, dynamic excitation is turned off at the estimated time interval and the soil was allowed to vibrate freely. Finally, before starting the dynamic analysis, the nodal points were selected at the required positions over the surface of the foundation bed. It helps to measure the dynamic response the foundation bed under the applied dynamic excitation. Initially, the numerical models were systematically validated with the results obtained from the field studies. The experimental results of geocell reinforced conditions were compared with the two modelling approaches, namely, ECA and HSA. Further, the validated numerical model was used to investigate the influence of various reinforcement parameters on the performance of geocell reinforced machine foundation bed.

4. Results and discussion

The variation of the displacement amplitude with the frequency obtained from the experimental and numerical study for different reinforced conditions is shown in Fig. 10. From the figure, it was observed that the resonant amplitude of foundation bed was significantly reduced in the presence of geocell reinforcement. In the presence of geocell, 56% reduction in the displacement amplitude was observed as compared to the unreinforced condition. Similarly, 42% change of resonant frequency was observed in the presence of geocell reinforcement. The all-round confinement offered by geocell reinforcement is the reason for the improvement in the frequency and the reduction in amplitude of the system. The experimental results of unreinforced condition have shown good agreement with the numerical results. Further, it was observed that the approach used for modelling the geocell reinforcement plays a prominent role in obtaining the actual response of a geocell reinforced system. It is evident from Fig. 10 that the HSA provides a good estimation of the experimental results as compared to the ECA. The ECA was found to overestimate the behaviour of geocell reinforced condition. As compared to the experimental results, the ECA overestimated the change of resonant frequency and the reduction in displacement amplitude by 4% and 10% respectively.

The change in amplitude of the vibration of the soil particles with respect to time was quantified in terms of Peak Particle Velocity (PPV). It signifies the maximum velocity attained by the soil grains due to the transmission of induced vibration energy through the foundation bed. The accelerometer was used to measure the velocity attained by the soil particles due to the machine induced vibration. It is capable to measure the velocity up to 200 mm/s with the resolution of 0.1 mm/s. Primarily, the accelerometer positions were predetermined and marked over the ground surface from the vibration source. The base of the accelerometer was made to rest over the ground surface. The other end was connected to the vibration meter. It helps to record the vibration pick ups received from the accelerometer in terms of velocity. Total, four accelerometers were placed at the intervals of 0.5 m from the vibration source to measure the variation in PPV of different conditions. The comparison between the variation in peak particle velocity observed from the experimental and numerical studies for different reinforced conditions is shown in Fig. 11. From the figure, about 49% reduction in PPV was observed in the presence of geocell at 0.5 m distance, as compared to the unreinforced condition. The PPV values estimated from the numerical simulations have shown a good agreement with the experimental findings. The HSA provided the realistic estimation of PPV than the ECA.

The area surrounded by the vibration source may get affected by the spreading of induced vibrations from the oscillator. The distribution of the emanated energy was studied in the form of displacement contours. The variation in the lateral spreading of emanated vibrations from the machine source for different reinforced conditions is shown in Fig. 12. The presented results are corresponding to their respective resonant frequencies. From the figure, the maximum lateral spreading was observed in the case of the unreinforced condition. However, it was significantly reduced in the presence of geocell reinforced condition due to the better energy absorption. The provision of geocells leads to an increment in the confinement area which further results in better absorption of emanated energy. From the figure, it was observed that the lateral spreading of the displacement was less in ECA as compared to the HSA. The distribution of displacement contours was extended up to $6.5B$ and $8.0B$ from the source in the ECA and HSA techniques respectively. The overestimation of the natural frequency of the foundation soil system in the ECA is the reason for observing lesser displacement values.

Further, the improvement in the dynamic properties of the foundation bed in the presence of geocells was investigated. The results of the two modelling techniques were compared with the experimental results. The dynamic properties studied in the present study include the dynamic elastic constants, stiffness and the shear modulus of the system. The considered dynamic elastic constants include coefficient of elastic uniform compression (C_u), coefficient of elastic uniform shear (C_τ), coefficient of elastic non-uniform compression (C_ϕ), and coefficient of elastic non-uniform shear (C_Ψ). The improvement in elasticity of the soil in the presence of reinforcement was studied in terms of coefficient of elastic uniform compression (C_u). It can be determined by,

$$C_u = 4\pi^2 f_{nz}^2 \frac{M}{A} \tag{9}$$

where M is the total mass of the concrete block and oscillator assembly, A is the contact area of the block with the soil and f_{nz} is the natural frequency of the foundation soil system. The coefficient of elastic uniform compression is the ratio of external uniform pressure in vertical direction to the elastic part of the vertical settlement. It represents the

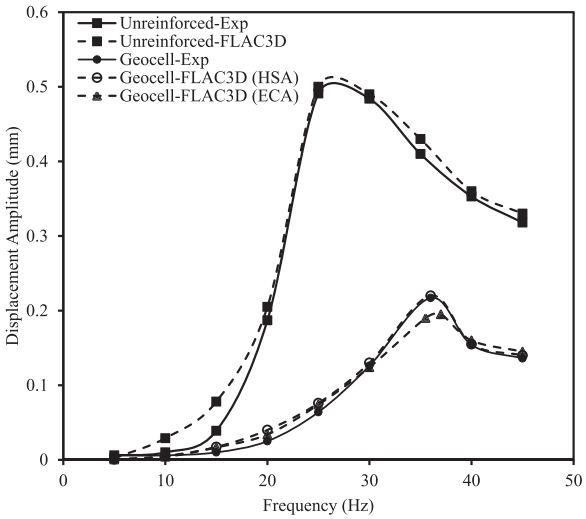

Fig. 10. Comparison of displacement amplitude-frequency behaviour obtained from experimental and numerical studies.

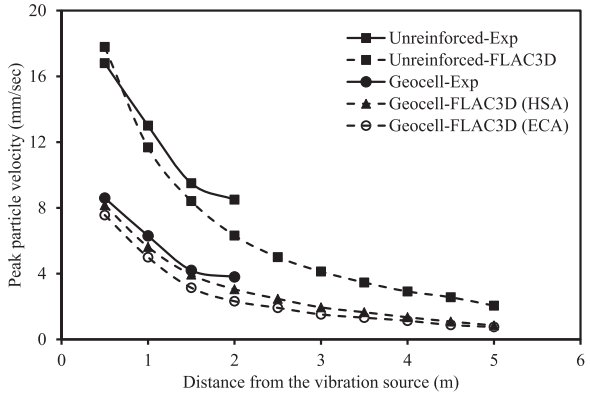

Fig. 11. Comparison of the change in PPV with the distance obtained from the experimental and numerical studies.

coefficient of subgrade reaction of the soil in vertical deformation mode. From the obtained C_u value, the remaining dynamic elastic constants, namely, C_τ, C_ϕ, and C_Ψ were determined based on the following relationships suggested by the Barkan [64].

$$C_\tau = 0.5 \quad C_u \tag{10}$$

$$C_\phi = 2C_u \tag{11}$$

$$C_\Psi = 0.75 \quad C_u \tag{12}$$

These parameters represent the deformation modes in uniform shear, non-uniform compression and non-uniform shear directions respectively. The stiffness of the reinforced foundation bed was calculated by multiplying the contact area of the block with the soil and the coefficient of elastic uniform compression. The shear modulus (G) of the soil was determined by using the following equation as suggested by Lysmer [65].

$$G = \frac{K(1-\nu)}{4r_0} \tag{13}$$

$$r_0 = \sqrt{A/\pi} \tag{14}$$

where K is the soil stiffness, ν is the Poisson's ratio of the soil and r_0 is the equivalent radius of the non-circular footing.

The variation in dynamic elastic constants for different reinforced conditions is shown in Fig. 13(a). Similarly, the variation in stiffness and shear modulus of the reinforced beds is shown in Fig. 13(b). It is evident from Fig. 13 that the ECA overestimated the dynamic properties of the foundation bed. The dynamic elastic constants and the shear modulus were overestimated by around 9% in the ECA as compared to the experimental values. On the other hand, the HSA provided a realistic estimation of these dynamic properties with the variation of around 3%. Hence, HSA was used for further analysis to understand the influence of various geocell properties on the dynamic response of the reinforced foundation bed.

As a result of the machine loading, the reinforcement undergoes considerable amount of deformation. Hence, in this study, the variation in the deformation profile of the reinforcement along its length has been investigated. The variation in the deformation profile of the geocell reinforcement is shown in Fig. 14. The presented deformation is corresponding to the resonant frequency of the geocell reinforced condition. The deformation of the geocell was observed at three different locations namely, at A-A (centre), 0.5 m (B-B), and 1 m (C-C) from the centre to both sides of the reinforcement. From the figure, it was observed that the maximum displacement in the reinforcement occurred at its centre and it decreases with the increase in distance from the centreline of reinforcement.

The effect of normalized cell depth (H/B) and normalized pocket diameter (d/B) of the geocell on the isolation of vibration was investigated. The H/B and d/B used in the experimental investigation are 0.2 and 0.42 respectively. The isolation efficiency of the cellular confinement system was studied in terms of Amplitude reduction ratio (A_{rf}). The A_{rf} is the ratio between the displacement amplitude of the reinforced system to that of the unreinforced system. It should be lowest for better isolation system. The variation in amplitude reduction ratio with the change in the normalized cell depth and diameter is shown in Fig. 15a. From the figure, it can be observed that the amplitude reduction ratio reduces with an increase in the cell depth for the irrespective of the pocket size. Moreover, for a constant value of cell depth, the A_{rf} was found to increase with an increase in pocket size. The rate of reduction in A_{rf} was found minimum beyond the cell depth of 0.25B. Hence, 0.25B was considered as the optimum cell height for the effective screening of the amplitude of vibrations. Further, the screening efficiency was found to increase with the decrease in normalized pocket diameter.

Similarly, the change of resonant frequency with the change in normalized cell depth and diameter was studied in terms of Frequency improvement ratio (F_{ir}). It represents the change in resonant frequency of the foundation soil system in the presence of reinforcement. The F_{ir} can be defined as,

$$F_{ir} = \frac{F_r}{F_u} \tag{15}$$

where F_r is the resonant frequency of the reinforced soil system, and F_u is the natural frequency of the unreinforced soil system at the resonance condition. The variation in frequency improvement ratio with the change in normalized cell depth and diameter is shown in Fig. 15b. From the figure, it was observed that the F_{ir} increased with an increase in cell depth for all the values of the normalized pocket diameter. Further, maximum rate of improvement in F_{ir} was observed with the decrease in normalized pocket diameter at the cell depth of 0.25B. Overall, the minimum cell diameter with the cell depth of 0.25B is suitable for the effective isolation of machine induced vibrations and changing the resonant frequency of a system.

On the other hand, the effect of damping is significant when the foundations are resting over the existing soil surface [73,74]. In the present study, the effect of geocell in improving the damping ratio of foundation bed was investigated. The damping ratio (ξ) is defined as the ratio between the damping coefficient of the reinforced system to the damping coefficient of unreinforced system. Mathematically,

$$\xi = \frac{\zeta_R}{\zeta_U} \tag{16}$$

where ζ_U and ζ_R are the damping coefficients of the unreinforced and geocell reinforced soil systems respectively. The damping coefficient (ζ) under vertical mode of vibration can be determined by using the following equation as suggested by Hardin and Drnevich [82].

$$\zeta = \frac{3.4 \quad r_0^2\sqrt{G\rho}}{1-\upsilon} \tag{17}$$

where ϑ, G and ρ are the Poisson's ratio, shear modulus and density of the soil respectively, and r_o is the equivalent radius of the circular foundation. The shear modulus of the soil can be calculated by using the Eq. (13) as mentioned in the original manuscript. From the Eq. (16), the damping ratio for the unreinforced condition is one. Whereas, it was observed as 1.42 in the case of geocell reinforced condition. It indicates that the improvement in damping ratio of the foundation bed in the presence of geocell reinforcement. The improvement in damping ratio is contributed of two parts, namely, material and radiation damping. The material damping is due to the hysteresis effect of soil under loading condition. Whereas, the radiation damping is due to the dissipation of emanated vibration energy by radiation process.

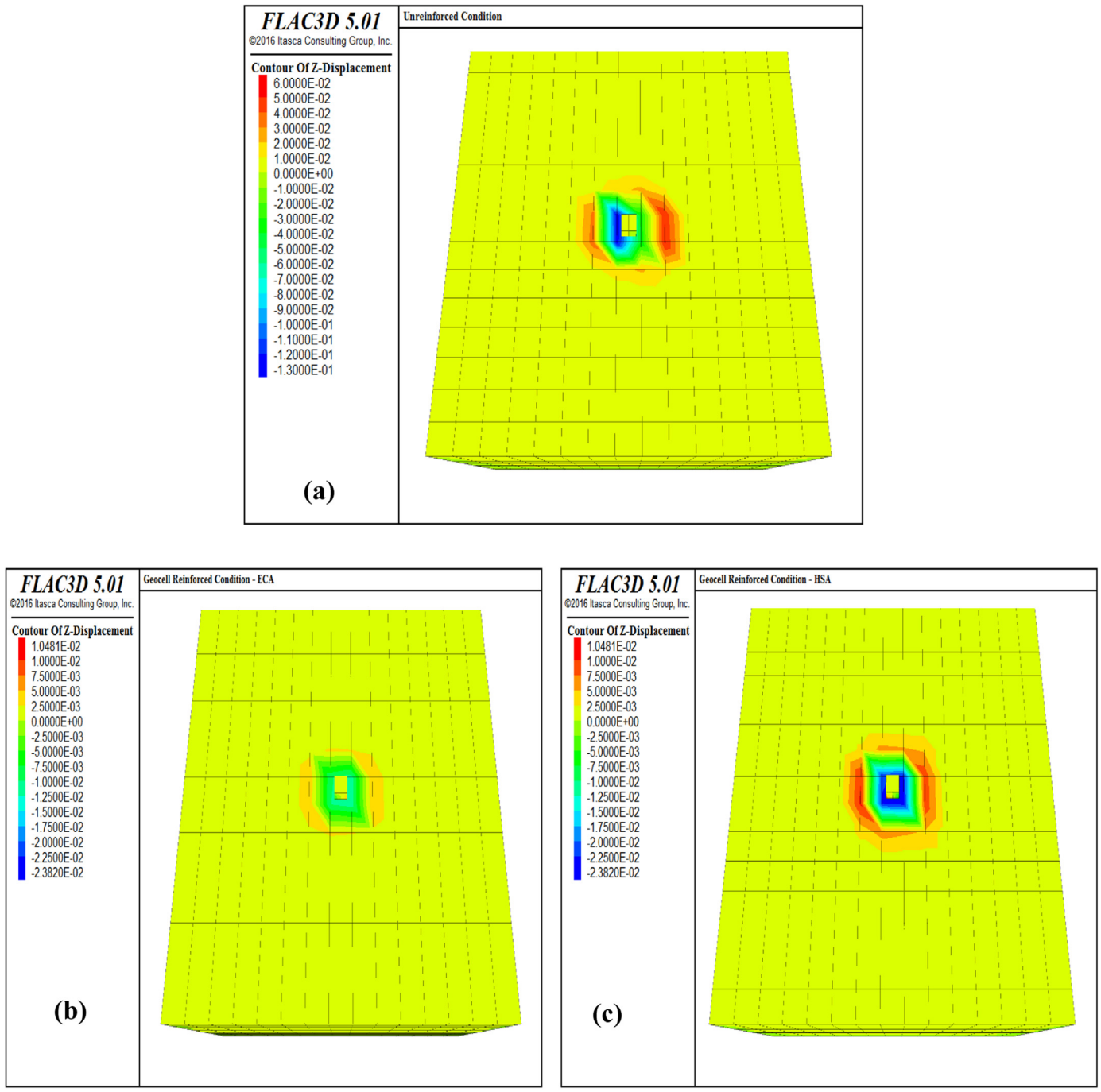

Fig. 12. Displacement contours: (a) unreinforced; (b) geocell reinforced-ECA; (c) geocell reinforced-HSA.

4.1. Factors affecting the dynamic response of cellular confinement cells

With an increase in the number of manufacturing companies, a wide variety of cellular confinement products are available in the market. There is a significant deviation in the geometry and strength properties from one product to another. The performance of the reinforced foundation bed gets influenced by the change in properties of the reinforcement material. In this section, the effect of various geocell properties on the dynamic response of geocell reinforced soil system has been investigated through the validated numerical model. The different geocell properties considered are, (i) elastic modulus of the geocell; (ii) interface friction angle; (iii) depth of placement; and (iv) width of the geocell mattress.

The modulus of the geocell used in the baseline case (experimental study) was 275 MPa. To understand the effect of change in the geocell modulus value, two lower and two higher values were selected. The modulus of the geocell was changed to one-fourth (i.e., 68.75 MPa), half (i.e., 137.5 MPa), twice (i.e., 550 MPa) and four times (i.e., 1100 MPa) of its original value. The variation in displacement amplitude-frequency behaviour of geocell reinforced bed with the change in the geocell modulus is shown in Fig. 16a. From the figure, it was observed that with an increase in geocell modulus, the natural frequency (f_{nz}) of the foundation bed was improved and the resonant amplitude (X_m) was reduced. Hegde and Sitharam [34,45] have also observed that the geocell modulus directly influences the performance of the foundation bed under static loading conditions.

The interface friction angle for the NPA geocell used in the experimental study was 30° as estimated from the modified direct shear

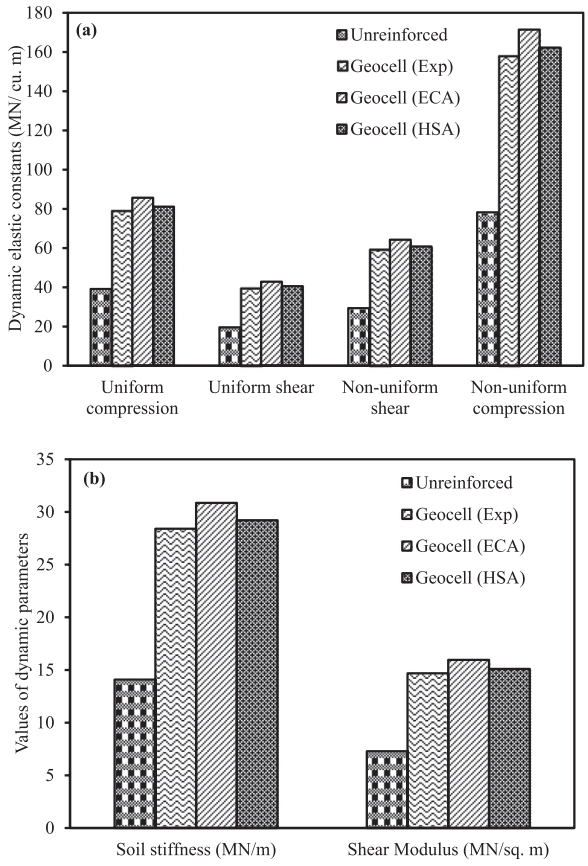

Fig. 13. Variation in (a) dynamic elastic constants; (b) dynamic properties of the foundation bed for different reinforced conditions.

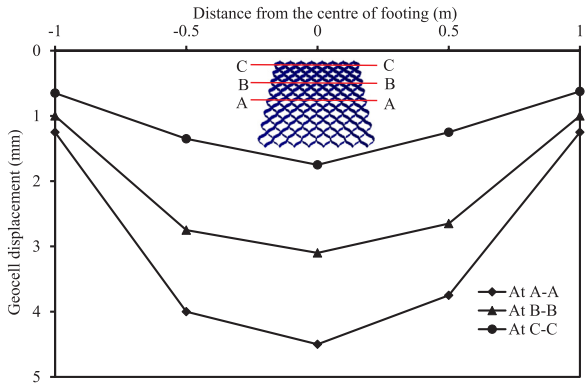

Fig. 14. Deformation profile of the geocell reinforcement.

test. The rough texture on the surface of the NPA geocell and the silty sand infill material account for such high interface friction value. The interface friction angle would change with variation in the surface texture and infill material. The various interface friction angle values considered for the parametric analysis are 22°, 26°, and 34°. Fig. 16b shows the displacement amplitude-frequency behaviour of the geocell reinforced foundation bed for different interface friction angles. From the figure, a reduction in displacement amplitude (X_m) and an change in natural frequency (f_{nz}) of the foundation soil system was observed with an increase in interface friction angle. This improved performance of foundation bed is attributed due to the increase in friction force developed between the infill material and the inner surface of the geocell. The induced friction force will act in the opposite direction, thus resulting in a reduction in displacement amplitude.

The geocell was placed at a depth of 0.1*B* in the experimental study

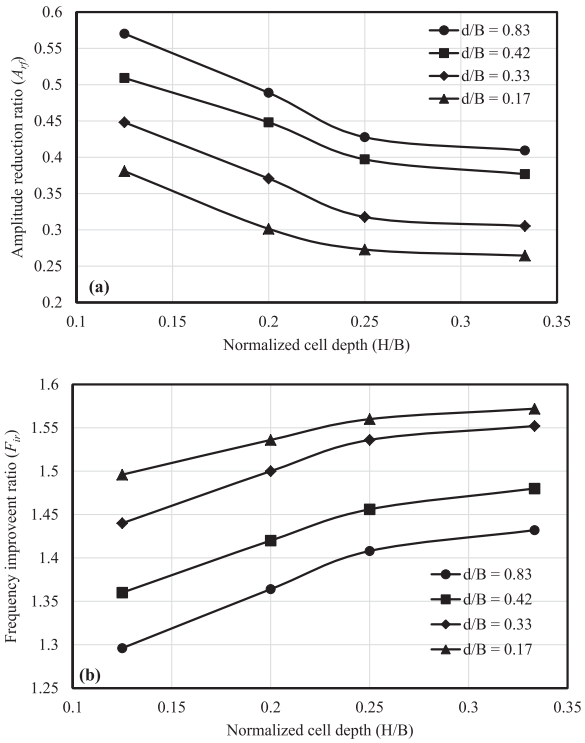

Fig. 15. Variation in (a) amplitude reduction ratio; (b) frequency improvement ratio with the change in normalized cell depth and the diameter of geocell reinforcement.

(where *B* is the width of the machine foundation). For the parametric analysis, the depth of placement (u_c) of the geocell was varied from 0.1*B* to 0.3*B* with an increment of 0.1*B* from the ground surface. The placement of geocell mattress directly on the ground surface (i.e. at 0*B*) is not practically feasible. A minimum soil cover is always essential to avoid the distortion of geocell reinforcement. Fig. 16c represents the variation in displacement amplitude-frequency behaviour with the change in depth of placement of geocell under the machine foundation. From the results, it was observed that the amplitude of vibration increases with an increase in the placement depth beyond 0.1*B*. Hence, 0.1*B* was considered as an optimum depth of placement of the geocell mattress for the effective improvement of the machine foundation behaviour.

The width of the geocell mattress used in the experimental study was 2 m (3.33*B*). For the parametric study, the width of the geocell was varied between 1 m (i.e., 1.67*B*) and 4 m (i.e., 6.67*B*) at the optimum depth of placement of geocell reinforcement. Fig. 16d shows the variation in displacement amplitude vs. frequency behaviour with the change in the width of the geocell mattress. The performance of geocells was improved with an increase in its width. With the increase in width of the geocell mattress, the emanated vibrations scatter through a wider area. It has led to a reduction in vibration amplitude. With the increase in geocell width, the number of cells under the footing was also increased, thus resulting in further densification of the foundation soil mass. Hence, the performance of the foundation bed was directly influenced by the width of the geocell mattress. The performance of the foundation bed significantly improved up to a width of 5*B*. The improvement was found marginal when the width of the geocell mattress increased beyond 5*B*. Hence, the optimum width of the geocell mattress was considered as 5*B*.

Further, the influence of geocell properties on the dynamic properties of the reinforced foundation bed was investigated. The variation in the dynamic properties with the change in geocell properties are summarized in Table 3. The dynamic properties were significantly improved with an increase in modulus, interface friction angle, and

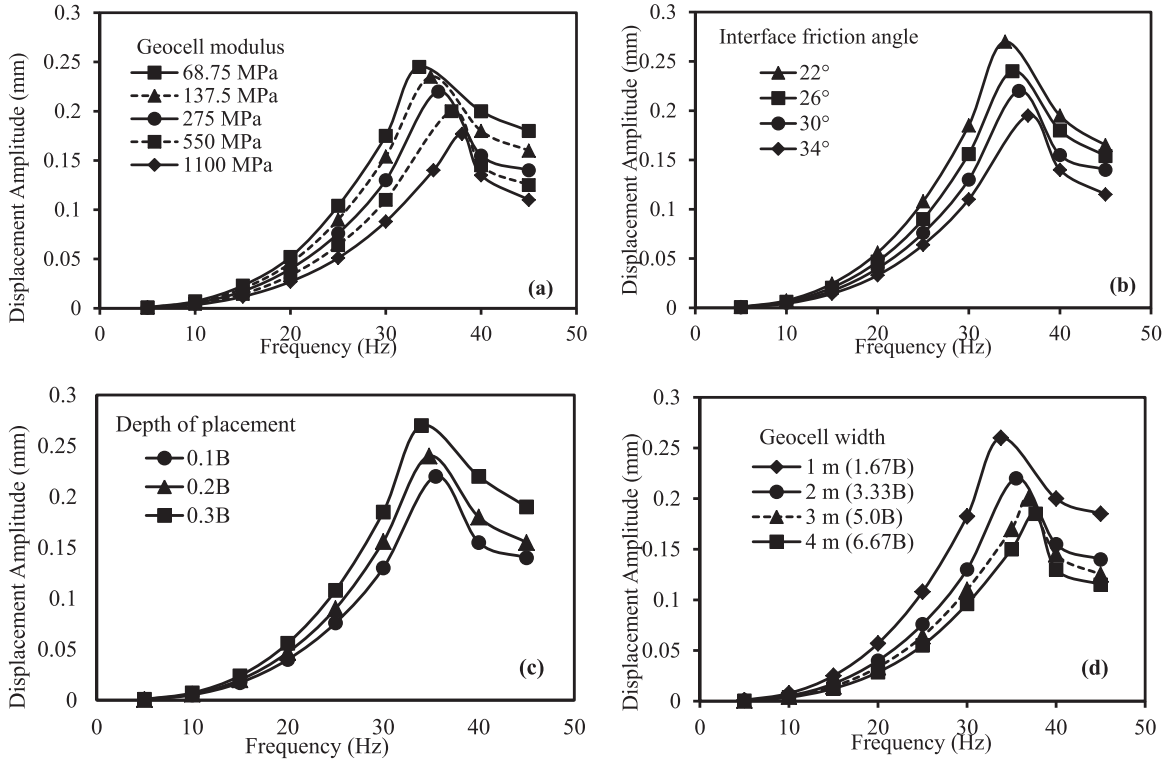

Fig. 16. Variation of displacement amplitude-frequency response with change in different geocell parameters: (a) modulus; (b) interface friction angle; (c) depth of placement; (d) width of the geocell mattress.

width of the geocell mattress.

5. Conclusions

The numerical simulation technique was successfully demonstrated to understand the effectiveness of the cellular confinement systems in isolating the machine induced vibrations. The developed numerical models were initially validated with the results of large-scale block resonance tests conducted over the unreinforced and geocell reinforced conditions. From the results, it was observed that the displacement amplitude was reduced by 56% in the presence of geocell reinforcement. Similarly, 42% change of resonant frequency of the unreinforced foundation bed was observed. In the presence of geocell reinforcement, the PPV was reduced by 49% at 0.5 m distance from the vibration source. The performance of geocell reinforced condition was predicted through two different numerical approaches, namely, ECA and HSA. Geocell modelled through the HSA has shown good agreement with the experimental results as compared to the ECA. The ECA was found to overestimate the improvement in resonant frequency and the reduction in amplitude by 4% and 10% respectively. The numerical results based on the HSA revealed that the minimum cell depth of 0.25*B* with a smaller geocell pocket diameter can provide better isolation

Table 3
Dynamic properties of the foundation bed for the different values of geocell properties.

Parameters		Resonant frequency, f_r (Hz)	Resonant amplitude, X_m (mm)	Dynamic properties of foundation bed				
				Coefficient of elastic uniform compression, C_u (MN/m^3)	Coefficient of elastic uniform shear, C_τ (MN/m^3)	Coefficient of elastic non-uniform shear, C_Ψ (MN/m^3)	Coefficient of elastic non-uniform compression, C_φ (MN/m^3)	Soil stiffness, K (MN/m)
Modulus of geocell, E (MPa)	68.7	33.5	0.24	70.3	35.1	52.7	140.5	25.3
	137.5	34.7	0.23	75.4	37.7	56.5	150.8	27.1
	275	36.0	0.22	81.1	40.6	60.8	162.3	29.2
	550	36.9	0.20	85.2	42.6	63.9	170.5	30.7
	1100	38.0	0.18	90.4	45.2	67.8	180.8	32.5
Interface friction angle, φ_i (°)	22	34.0	0.27	72.4	36.2	54.3	144.7	26.1
	26	34.8	0.24	75.8	37.9	56.9	151.6	27.3
	30	36.0	0.22	81.1	40.6	60.8	162.3	29.2
	34	36.5	0.19	83.4	41.7	62.6	166.8	30.0
Depth of placement of geocell, u_c (m)	0.1*B*	36.0	0.22	81.1	40.6	60.8	162.3	29.2
	0.2*B*	34.8	0.24	75.8	37.9	56.9	151.6	27.3
	0.3*B*	34.0	0.27	72.4	36.2	54.3	144.7	26.1
Width of geocell (m)	1	33.8	0.26	71.5	35.8	53.6	143.0	25.8
	2	36.0	0.22	81.1	40.6	60.8	162.3	29.2
	3	36.9	0.20	85.2	42.6	63.9	170.5	30.7
	4	37.7	0.18	89.0	44.5	66.7	178.0	32.0

performance. The results of the parametric studies revealed that the modulus and the interface friction angle directly influence the performance of geocell reinforced foundation beds.

References

[1] Woods RD. Screening of surface waves in soils. J Soil Mech Found Div 1968;94:951–79.
[2] Gao GY, Li ZY, Qiu C, Yue ZQ. Three-dimensional analysis of rows of piles as passive barriers for ground vibration isolation. Soil Dyn Earthq Eng 2006;26(11):1015–27. https://doi.org/10.1016/j.soildyn.2006.02.005.
[3] Gao G, Chen J, Gu X, Song J, Li S, Li N. Numerical study on the active vibration isolation by wave impeding block in saturated soils under vertical loading. Soil Dyn Earthq Eng 2017;93:99–112. https://doi.org/10.1016/j.soildyn.2016.12.006.
[4] Ahmad S, Al-Hussaini TM, Fishman KL. Investigation on active isolation of machine foundations by open trenches. J Geotech Eng 1996;122(6):454–61. https://doi.org/10.1061/(ASCE)0733-9410(1996)122:6(454).
[5] Klein R, Antes H, Le Houédec D. Efficient 3D modelling of vibration isolation by open trenches. Comput Struct 1997;64(1–4):809–17. https://doi.org/10.1016/S0045-7949(96)00418-X.
[6] Alzawi A, El Naggar MH. Full scale experimental study on vibration scattering using open and in-filled (GeoFoam) wave barriers. Soil Dyn Earthq Eng 2011;31(3):306–17. https://doi.org/10.1016/j.soildyn.2010.08.010.
[7] Ju SH. Three-dimensional analyses of wave barriers for reduction of train-induced vibrations. J Geotech Geoenviron Eng 2004;130(7):740–8. https://doi.org/10.1061/(ASCE)1090-0241(2004)130: 7(740).
[8] Adam M, Von Estorff O. Reduction of train-induced building vibrations by using open and filled trenches. Comput Struct 2005;83(1):11–24. https://doi.org/10.1016/j.compstruc.2004.08.010.
[9] Di Mino G, Giunta M, Di Liberto CM. Assessing the open trenches in screening railway ground-borne vibrations by means of artificial neural network. Adv Acoust Vib 2009:2009. https://doi.org/10.1155/2009/942787.
[10] Saikia A, Das UK. Analysis and design of open trench barriers in screening steady state surface vibrations. Earthq Eng Eng Vib 2014;13(3):545–54. https://doi.org/10.1007/s11803-014-0261-x.
[11] Kumar P, Sandhu HK, Chakraborty SK. Isolation of plane shear wave using water saturated trench barrier. Soil Dyn Earthq Eng 2014;59:42–50. https://doi.org/10.1016/j.soildyn.2014.01.004.
[12] Coulier P, Cuéllar V, Degrande G, Lombaert G. Experimental and numerical evaluation of the effectiveness of a stiff wave barrier in the soil. Soil Dyn Earthq Eng 2015;77:238–53. https://doi.org/10.1016/j.soildyn.2015.04.007.
[13] Thompson DJ, Jiang J, Toward MGR, Hussein MFM, Ntotsios E, Dijckmans A, et al. Reducing railway-induced ground-borne vibration by using open trenches and soft-filled barriers. Soil Dyn Earthq Eng 2016;88:45–59. https://doi.org/10.1016/j.soildyn.2016.05.009.
[14] Bordón JDR, Aznárez JJ, Schevenels M, Maeso O, Lombaert G. Shape optimized inclined single and double wall wave barriers for ground vibration mitigation. Soil Dyn Earthq Eng 2018;112:215–31. https://doi.org/10.1016/j.soildyn.2018.04.035.
[15] Psyrras NK, Sextos AG. Safety of buried steel natural gas pipelines under earthquake-induced ground shaking: a review. Soil Dyn Earthq Eng 2018;106:254–77. https://doi.org/10.1016/j.soildyn.2017.12.020.
[16] Pu X, Shi Z, Xiang H. Feasibility of ambient vibration screening by periodic geofoam-filled trenches. Soil Dyn Earthq Eng 2018;104:228–35. https://doi.org/10.1016/j.soildyn.2017.10.022.
[17] Yang YB, Ge P, Li Q, Liang X, Wu Y. 2.5 D vibration of railway-side buildings mitigated by open or infilled trenches considering rail irregularity. Soil Dyn Earthq Eng 2018;106:204–14. https://doi.org/10.1016/j.soildyn.2017.12.027.
[18] Beskos DE, Dasgupta B, Vardoulakis IG. Vibration isolation using open or filled trenches Part 1: 2-D homogeneous soil. Comput Mech 1986;1(1):43–63. https://doi.org/10.1007/BF00298637.
[19] Dasgupta B, Beskos DE, Vardoulakis IG. Vibration isolation using open or filled trenches Part 2: 3-D homogeneous soil. Comput Mech 1990;6(2):129–42. https://doi.org/10.1007/BF00350518.
[20] Al-Hussaini TM, Ahmad S. Design of wave barriers for reduction of horizontal ground vibration. J Geotech Eng 1991;117(4):616–36. https://doi.org/10.1061/(ASCE)0733-9410(1992)118:8(1280).
[21] Yang YB, Hung HH. A parametric study of wave barriers for reduction of train-induced vibrations. Int J Numer Methods Eng 1997;40(20):3729–47. https://doi.org/10.1002/(SICI)1097-0207(19971030)40:20<3729::AID-NME236>3.0.CO;2-8.
[22] Hung HH, Yang YB, Chang DW. Wave barriers for reduction of train-induced vibrations in soils. J Geotech Geoenviron Eng 2004;130(12):1283–91. https://doi.org/10.1061/(ASCE)1090-0241(2004)130:12(1283).
[23] Al-Hussaini TM, Ahmad S. Active isolation of machine foundations by in-filled trench barriers. J Geotech Eng 1996;122(4):288–94. https://doi.org/10.1061/(ASCE)0733-9410(1996)122:4(288).
[24] Ashmawy AK, Bourdeau PL. Geosynthetic-reinforced soils under repeated loading: a review and comparative design study. Geosynth Int 1995;2(4):643–78. https://doi.org/10.1680/gein.2.0029.
[25] Ling HI, Liu H, Kaliakin VN, Leshchinsky D. Analyzing dynamic behavior of geosynthetic-reinforced soil retaining walls. J Eng Mech 2004;130(8):911–20. https://doi.org/10.1061/(ASCE)0733-9399(2004)130:8(911).
[26] Hegde A, Sitharam TG. Behaviour of geocell reinforced soft clay bed subjected to incremental cyclic loading. Geomech Eng 2016;10(4):405–22. https://doi.org/10.12989/gae.2016.10.4.405.
[27] Hegde A. Geocell reinforced foundation beds-past findings, present trends and future prospects: a state-of-the-art review. Constr Build Mater 2017;154:658–74. https://doi.org/10.1016/j.conbuildmat.2017.07.230.
[28] Boominathan S, Senathipathi K, Jayaprakasam V. Field studies on dynamic properties of reinforced earth. Soil Dyn Earthq Eng 1991;10(8):402–6. https://doi.org/10.1016/0267-7261(91)90054-4.
[29] Clement S, Sahu R, Ayothiraman R, Ramana, GV. Experimental studies on dynamic response of a block foundation on sand reinforced with geogrid. In: Proceedings of geosynthetics 2015. Portland, Oregon; 2015, p. 479–88.
[30] Sreedhar MVS, Abhishek J. Effect of geosynthetic reinforcement on dynamic characteristics through model block resonance tests. In: Proceedings of Indian geotechnical conference-2016. Chennai; 2016.
[31] Azzam WR. Utilization of the confined cell for improving the machine foundation behavior-numerical study. J GeoEng 2015;10(1):17–23. https://doi.org/10.6310/jog.2015.10(1).3.
[32] Venkateswarlu H, Hegde A. Dynamic response of the machine foundation resting on geocell reinforced soil beds. In: Proceedings of Indian geotechnical conference-2017. Guwahati; 2017, Paper ID Th11-559.
[33] Hegde A, Sitharam TG. 3-dimensional numerical modelling of geocell reinforced sand beds. Geotext Geomembr 2015;43:171–81. https://doi.org/10.1016/j.geotexmem.2014.11.009.
[34] Hegde AM, Sitharam TG. Effect of infill materials on the performance of geocell reinforced soft clay beds. Geomech Geoengin 2015;10(3):163–73. https://doi.org/10.1080/17486025.2014.921334.
[35] Bathurst RJ, Karpurapu R. Large-scale triaxial compression testing of geocell-reinforced granular soils. Geotech Test J 1993;16(3):296–303. https://doi.org/10.1520/GTJ10050J.
[36] Rajagopal K, Krishnaswamy NR, Latha GM. Behaviour of sand confined with single and multiple geocells. Geotext Geomembr 1999;17(3):171–84. https://doi.org/10.1016/S0266-1144(98)00034-X.
[37] Latha GM, Somwanshi A. Effect of reinforcement form on the bearing capacity of square footings on sand. Geotext Geomembr 2009;27(6):409–22. https://doi.org/10.1016/j.geotexmem.2009.03.005.
[38] Mehdipour I, Ghazavi M, Moayed RZ. Numerical study on stability analysis of geocell reinforced slopes by considering the bending effect. Geotext Geomembr 2013;37:23–34. https://doi.org/10.1016/j.geotexmem.2013.01.001.
[39] Hegde A, Sitharam TG. Experimental and numerical studies on footings supported on geocell reinforced sand and clay beds. Int J Geotech Eng 2013;7(4):346–54. https://doi.org/10.1179/1938636213Z.00000000043.
[40] Han J, Yang X, Leshchinsky D, Parsons R. Behavior of geocell-reinforced sand under a vertical load. Transp Res Rec: J Transp Res Board 2008;2045:95–101. https://doi.org/10.3141/2045-11.
[41] Saride S, Gowrisetti S, Sitharam TG, Puppala AJ. Numerical simulation of geocell-reinforced sand and clay. Proc Inst Civ Eng-Ground Improv 2009;162(4):185–98. https://doi.org/10.1680/grim.2009.162.4.185.
[42] Leshchinsky B, Ling HI. Numerical modeling of behavior of railway ballasted structure with geocell confinement. Geotext Geomembr 2013;36:33–43. https://doi.org/10.1016/j.geotexmem.2012.10.006.
[43] Yang X, Han J, Parsons RL, Leshchinsky D. Three-dimensional numerical modeling of single geocell-reinforced sand. Front Archit Civ Eng China 2010;4(2):233–40. https://doi.org/10.1007/s11709-010-0020-7.
[44] Hegde AM, Sitharam TG. Experimental and numerical studies on protection of buried pipelines and underground utilities using geocells. Geotext Geomembr 2015;43(5):372–81. https://doi.org/10.1016/j.geotexmem.2015.04.010.
[45] Hegde AM, Sitharam TG. Three-dimensional numerical analysis of geocell reinforced soft clay beds by considering the actual geometry of geocell pockets. Can Geotech J 2015;52:1–12. https://doi.org/10.1139/cgj-2014-0387.
[46] ASTM D4885-01. Standard test method for determining performance strength of geomembranes by the wide strip tensile method. West Conshohocken, PA: ASTM International; 2018. https://doi.org/10.1520/D4885-01R182018. [2018].
[47] Gazetas G. Formulas and charts for impedances of surface and embedded foundations. J Geotech Eng 1991;117(9):1363–81. https://doi.org/10.1061/(ASCE)0733-9410(1991)117:9(1363).
[48] Skempton AW. Standard penetration test procedures and the effects in sands of overburden pressure, relative density, particle size, ageing and overconsolidation. Geotechnique 1986;36(3):425–47. https://doi.org/10.1680/geot.1986.36.3. 425.
[49] Mandal A, Baidya DK, Roy D. Dynamic response of the foundations resting on a two-layered soil underlain by a rigid layer. Geotech Geol Eng 2012;30(4):775–86. https://doi.org/10.1007/s10706-012-9497-2.
[50] Bowles LE. Foundation analysis and design. New York, USA: McGraw Hill; 1996.
[51] Tafreshi SM, Mehrjardi GT, Ahmadi M. Experimental and numerical investigation on circular footing subjected to incremental cyclic loads. Int J Civ Eng 2011;9(4):265–74.
[52] Sukmak K, Han J, Sukmak P, Horpibulsuk S. Numerical parametric study on behavior of bearing reinforcement earth walls with different backfill material properties. Geosynth Int 2016;23(6):435–51. https://doi.org/10.1680/jgein.16.00008.
[53] Navaratnarajah SK, Indraratna B, Ngo NT. Influence of under sleeper pads on ballast behavior under cyclic loading: experimental and numerical studies. J Geotech Geoenviron Eng 2018;144(9):1–16. https://doi.org/10.1061/(ASCE)GT.1943-5606.0001954.
[54] Richart FE, Hall JR, Woods RD. Vibrations of soils and foundations. International series in theoretical and applied mechanics. 1970.
[55] Biabani MM, Indraratna B, Ngo NT. Modelling of geocell-reinforced subballast subjected to cyclic loading. Geotext Geomembr 2016;44(4):489–503. https://doi.org/10.1016/j.geotexmem.2016.02.001.

[56] Yang X, Han J. Analytical model for resilient modulus and permanent deformation of geosynthetic-reinforced unbound granular material. J Geotech Geoenviron Eng 2012;139(9):1443–53. https://doi.org/10.1061/(ASCE)GT.1943-5606.0000879.
[57] Indraratna B, Biabani MM, Nimbalkar S. Behavior of geocell-reinforced subballast subjected to cyclic loading in plane-strain condition. J Geotech Geoenviron Eng 2014;141(1):04014081. https://doi.org/10.1061/(ASCE)GT.1943-5606.0001199.
[58] Henkel DJ, Gilbert GD. The effect measured of the rubber membrane on the triaxial compression strength of clay samples. Geotechnique 1952;3(1):20–9. https://doi.org/10.1680/geot.1952.3.1.20.
[59] Bathurst RJ, Knight MA. Analysis of geocell reinforced-soil covers over large span conduits. Comput Geotech 1998;22(3–4):205–19. https://doi.org/10.1016/S0266-352X(98)00008-1.
[60] Madhavi Latha G, Rajagopal K. Parametric finite element analyses of geocell-supported embankments. Can Geotech J 2007;44(8):917–27. https://doi.org/10.1139/T07-039.
[61] IS 456. Code of practice for plain and reinforced concrete. New Delhi, India: Bureau of Indian Standards; 2000.
[62] ASTM D5321/M-17 Standard Test Method for Determining the Shear Strength of Soil-Geosynthetic and Geosynthetic-Geosynthetic Interfaces by Direct Shear. West Conshohocken, PA: ASTM International; 2017. ⟨https://doi.org/10.1520/D5321_D5321M-17⟩.
[63] Itasca. Fast Lagrangian analysis of continua (FLAC^{3D} 5.01). Minneapolis, Minn: Itasca Consulting Group Inc.; 2008.
[64] Barkan DD. Dynamics of bases and foundations. New York, USA: McGraw Hill; 1962.
[65] Lysmer J. Vertical motions of rigid footings [Ph.D. Thesis]. AnnArbor: University of Michigan; 1965.
[66] Alpan I. The geotechnical properties of soils. Earth-Sci Rev 1970;6(1):5–49.
[67] Hegde A, Sitharam TG. Experiment and 3D-numerical studies on soft clay bed reinforced with different types of cellular confinement systems. Transp Geotech 2017;10:73–84.
[68] Alzawi A, El Naggar MH. Experimental investigations on vibration isolation using open and GeoFoam wave barriers: comparative study. In: Proceedings of the 63rd Canadian geotechnical conference. Calgary, AB, Canada; 2010, p. 360–8.
[69] Mbawala SJ. Behaviour of machine foundations subjected to vertical dynamic loading [Doctoral dissertation]. Pretoria, South Africa: University of Pretoria; 2015.
[70] Haldar S, Sivakumar Babu GL. Improvement of machine foundations using reinforcement. Proc Inst Civ Eng-Ground Improv 2009;162(4):199–204.
[71] Ghosh P. FLAC based numerical studies on dynamic interference of two nearby embedded machine foundations. Geotech Geol Eng 2012;30(5):1161–81.
[72] Venkateswarlu H, Ujjawal KN, Hegde A. Laboratory and numerical investigation of machine foundations reinforced with geogrids and geocells. Geotext Geomembr 2018;46(6):882–96.
[73] Baidya DK, Rathi A. Dynamic response of footings resting on a sand layer of finite thickness. J Geotech Geoenviron Eng 2004;130(6):651–5.
[74] Baidya DK, Mandal A. Dynamic response of footing resting on a layered soil system. West Indian J Eng 2006;28(2):65–79.
[75] Raman J. Dynamic response of footing soil system to vertical vibration [Ph.D. Thesis]. Bangalore, India: Indian Institute of Science; 1975.
[76] Kumar J, Reddy CO. Dynamic response of footing and machine with spring mounting base. Geotech Geol Eng 2006;24(1):15–27.
[77] Indian Standard Code 5249. Determination of dynamic properties of soil-method of test. 1992.
[78] Dash SK, Krishnaswamy NR, Rajagopal K. Bearing capacity of strip footings supported on geocell-reinforced sand. Geotext Geomembr 2001;19(4):235–56.
[79] Hegde A, Sitharam TG. Joint strength and wall deformation characteristics of a single cell geocell subjected to uniaxial compression. Int J Geomech 2015;15:1–8.
[80] Das BM. Principles of soil dynamics. Boston: PWS-KENT Publishing Company; 1992.
[81] Wichtmann T, Triantafyllidis T. On the correlation of “static” and “dynamic” stiffness moduli of non-cohesive soils. Bautechnik 2009;86(S1):S28–39.
[82] Hardin BO, Drnevich VP. Shear modulus and damping in soils: measurement and parameter effects. J Soil Mech Found Div 1972;98(sm6).